IEEE Access
Multidisciplinary | Rapid Review | Open Access Journal

Received February 16, 2021, accepted March 10, 2021, date of publication March 17, 2021, date of current version March 29, 2021.

Digital Object Identifier 10.1109/ACCESS.2021.3066444

Cascade Backstepping Control With Augmented Observer for Lateral Control of Vehicle

CHANG MOOK KANG[1], (Member, IEEE), WONHEE KIM[2], (Member, IEEE), AND HYEONGBOO BAEK[3]

[1]Department of Electrical Engineering, Incheon National University (INU), Incheon 22012, South Korea
[2]School of Energy Systems Engineering, Chung-Ang University, Seoul 06974, South Korea
[3]Department of Computer Science and Engineering, Incheon National University (INU), Incheon 22012, South Korea

Corresponding authors: Wonhee Kim (whkim79@cau.ac.kr) and Hyeongboo Baek (hbbaek@inu.ac.kr)

This work was supported in part by the Incheon National University (International Cooperative) Research Grant in 2020, and in part by the National Research Foundation of Korea (NRF) Grant by the Korean Government through Ministry of Science and ICT (MSIT) under Grant 2020R1F1A1071547.

ABSTRACT This paper proposes a cascaded backstepping control method with an augmented observer for the lateral control of an autonomous vehicle. The proposed cascaded backstepping control structure consists of an inner-loop electric power steering (EPS) system and an outer-loop lane-keeping system (LKS). The outer-loop controller for LKS calculates and provides the desired steering angle to the inner-loop EPS system for maintaining the vehicle at the center of the lane. Subsequently, the inner-loop controller for the EPS system generates steering torque to track the desired steering angle from the outer loop. The proposed method can guarantee the stability of the vehicle considering both inner-loop and outer-loop dynamics. In addition, an augmented observer affords robustness against unknown model parameters and external disturbances. The stability of the closed loop of the overall system, including the lateral dynamics and the EPS system, is proven using the input-to-state stable property. Controller design with consideration of the overall system can improve the lateral control performance.

INDEX TERMS Autonomous vehicle, backstepping control, lateral motion, state observer.

NOMENCLATURE

$\{XYZ\}$:	Local map coordinate frame
$\{xyz\}$:	Vehicle coordinate frame
V_x:	Longitudinal velocity at the center of gravity (c.g.) of the vehicle
m:	Total mass of the vehicle
I_z:	Yaw moment of the inertia of the vehicle
l:	(l_f, l_r) Longitudinal distance from c.g. to (front, rear) tires
α:	(α_f, α_r) Slip angle at (front, rear) tires
C_α:	$(C_{\alpha f}, C_{\alpha r})$ Cornering stiffness of (front, rear) tires
F_y:	(F_{yf}, F_{yr}) Lateral tire force on (front, rear) tires
e_y:	Lateral position error with respect to (w.r.t.) reference
$\dot{e}_y$:	Time derivative of lateral position error w.r.t. reference
$e_\psi = \psi^d - \psi$:	Yaw angle error with respect to road
ψ:	Yaw and heading angle of vehicle on global axis
$\dot{\psi}$:	Yaw rate of vehicle
δ:	Steering angle
θ_h:	Steering wheel angular position
θ_{h_d}:	Desired steering wheel angular position
ω_h:	Steering wheel angular velocity
θ_m:	Motor angular position
ω_m:	Motor angular velocity
i:	Current input of motor
T:	Input torque of system ($T = K_t i$)
T_{EPS}:	Drive-assistant torque
K_t:	Motor torque constant
T_d:	Driver torque
T_f:	Friction torque
T_r:	Road reaction torque on rack and pinion
J_c:	Steering column moment of inertia
B_c:	Steering column viscous damping
K_c:	Steering column stiffness
M_r:	Mass of rack

The associate editor coordinating the review of this manuscript and approving it for publication was Sara Dadras.

B_r: Viscous damping of rack
R_p: Radius of steering column pinion
K_r: Tire spring rate
J_m: Motor moment of inertia
B_m: Motor shaft viscous damping

I. INTRODUCTION

Advanced driver assistant systems (ADASs) provide ride comfort and stability for drivers. Recently, these ADASs have been developed and improved from driver assistance levels to vehicle control levels. In the vehicle-control-level ADASs, the control objective can be divided into two types: longitudinal and lateral motion. The longitudinal motion of a vehicle is controlled by considering engine dynamics and aerodynamics. The fuel efficiency of the vehicle's longitudinal safety from the front vehicle can be improved with longitudinal motion control. Therefore, many studies on longitudinal motion control have focused on fuel economy and maintaining a safe distance. A longitudinal controller featuring better properties than existing ones with respect to performance and impact on fuel economy and pollution during traffic disturbances was introduced in [1]. In [2], [3], a controller that guaranteed significant stability of vehicle platoons was presented. A decentralized controller design scheme with a limited communication structure for heterogeneous vehicles was proposed and validated in [4]. An adaptive cruise control (ACC) system that could address tracking capability and fuel economy was proposed in [5], [6].

The lateral control of a vehicle, instead of longitudinal control, is examined to ensure stability. The lateral control structure consists of an outer-loop (upper-level) controller for lateral dynamics and an inner-loop (lower-level) controller for the electric power steering (EPS) system. In the outer-loop controller, the desired steering angle is obtained to track the desired lateral position for the lateral position. Various methods have been studied for the outer-loop control. A linear quadratic controller and model predictive control method were previously proposed [7]–[9]. Fuzzy-logic-based lateral motion controllers were presented in [10]–[12]. An online estimation of inertial parameters was proposed for lightweight electric vehicles by using a dual unscented Kalman filter approach [13]. In [14], a backstepping control scheme using a simple second-order model was introduced for LKS. In the outer loop (lateral dynamics), the steering angle is regarded as the system input, although the input torque is the actual input of the overall system. Thus, the desired steering angle is obtained by the outer-loop controller. Then, the steering angle is controlled to track the desired steering angle by using an inner-loop controller. In the inner-loop controller, the torque of the EPS system is calculated to track the desired steering angle.

Several methods have been proposed to improve the steering wheel tracking performance. A nonlinear hybrid impedance approach was proposed in [15]. In [16], a second-order sliding-mode controller with a fuzzy neural network was studied. A model predictive control approach for steering systems was proposed in [17]. Although these previous methods improved the control performance, only the outer loop or the inner loop was considered. In other words, the overall system, including the lateral dynamics and the EPS system, was not considered in the controller design. Because the previous outer-loop controller was designed without considering the inner-loop system (EPS system), the mismatch between the desired steer angle and the actual steering angle can result in poor lateral control performance. Thus, a control method for the overall system, including the lateral dynamics and the EPS system, is required to improve the lateral control performance. Recently, in [18], a two-layer controller approach for the lateral control of vehicles was proposed; however, the stability of the overall system was not mathematically proven.

In this paper, we propose a cascaded backstepping control method with an augmented observer for the lateral control of an autonomous vehicle. The proposed method is designed to improve the lateral control performance, while guaranteeing the stability of the overall system via a cascaded backstepping procedure. The proposed method consists of an outer-loop controller and an inner-loop controller. The outer-loop controller calculates the desired steering angle for lateral control in lateral dynamics. From the inner-loop controller, the torque of the EPS system required to track the desired steering angle is obtained. Augmented observers are designed to estimate the complete state and disturbances, including unknown model parameters and external disturbances. Accordingly, augmented observers are implemented in the outer-loop and inner-loop controllers to improve the robustness against unknown model parameters and external disturbances. The stability of the closed loop of the overall system is proven using the input-to-state stable property. Controller design with consideration of the overall system can improve the lateral control performance. The control performance of the proposed controller is validated via the vehicle dynamic simulator CarSim and MATLAB/Simulink. In the simulation, the proposed cascaded backstepping approach for a hierarchical system exhibits a stable and reasonable lane-keeping performance, even in the presence of unknown disturbances.

II. CASCADE BACKSTEPPING CONTROLLER

A. CONTROLLER

Let us consider second-order dynamics given by

$$\begin{aligned} \dot{x}_1 &= x_2 \\ \dot{x}_2 &= gu + d \end{aligned} \tag{1}$$

where d denotes an unknown disturbance including uncertain system parameters, g is a system parameter, and u is the control input. Now, let us define the tracking error as

$$\begin{aligned} e_1 &= x_1 - x_{1_d} \\ e_2 &= x_2 - x_{2_d}. \end{aligned} \tag{2}$$

Then, we can represent the tracking error dynamics as follows:

$$\begin{aligned}\dot{e}_1 &= e_2 + x_{2_d} - \dot{x}_{1_d}\\ \dot{e}_2 &= gu + d - \dot{x}_{2_d}.\end{aligned} \tag{3}$$

The control input u and the desired value of the second state x_{2_d} can be designed as follows to guarantee stability:

$$\begin{aligned}x_{2d} &= -k_1 e_1 + \dot{x}_{1_d}\\ u &= \frac{1}{g}\left(-k_2 e_2 + \dot{x}_{2_d} - \hat{d}\right)\end{aligned} \tag{4}$$

where k_1 and k_2 are positive constants, and $\hat{d}$ is the bounded disturbance estimated by the observer that is yet to be designed. When (4) is applied to (1), the error dynamics can be expressed as (5)

$$\begin{aligned}\dot{e}_1 &= -k_1 e_1 + e_2\\ \dot{e}_2 &= -k_2 e_2 + \tilde{d}.\end{aligned} \tag{5}$$

Theorem 1: The tracking error dynamics in equation (5) represent the serial interconnected system with the following input-to-stable (ISS) property such that

$$\begin{aligned}|e_1(t)| \; leq \; &\exp\left(-\frac{k_1}{2}t\right)|e_1(0)| + \frac{2}{k_1}\sup_{0\le\tau\le t}|e_2(\tau)|\\ |e_2(t)| \;\le\; &\exp\left(-\frac{k_2}{2}t\right)|e_2(0)| + \frac{2}{k_2}\sup_{0\le\tau\le t}|\tilde{d}(\tau)|.\end{aligned} \tag{6}$$

◇

Proof: From (5), the dynamics of e_2^2 are written as

$$\begin{aligned}\frac{d}{dt}\left(\frac{e_2^2}{2}\right) &= -k_2 e_2^2 + e_2\tilde{d}\\ &\le -\frac{k_2}{2}e_2^2 - \left(\frac{k_2}{2}\right)|e_2|\left(|e_2| - \frac{2}{k_2}|\tilde{d}|\right).\end{aligned} \tag{7}$$

Using Lemma 6.20 and Theorem C.2 in [19], we derive the following result:

$$|e_2(t)| \le \exp\left(-\frac{k_2}{2}t\right)|e_2(0)| + \frac{2}{k_2}\sup_{0\le\tau\le t}|\tilde{d}(\tau)|. \tag{8}$$

Equation (8) shows that the relationship between e_2 and $\tilde{d}$ has the ISS property. From (5), the dynamics of e_1^2 are obtained as

$$\begin{aligned}\frac{d}{dt}\left(\frac{e_1^2}{2}\right) &= -k_1 e_1^2 + e_1 e_2\\ &\le -\frac{k_1}{2}e_1^2 - \left(\frac{k_1}{2}\right)|e_1|\left(|e_1| - \frac{2}{k_1}|e_2|\right).\end{aligned} \tag{9}$$

Then,

$$|e_1(t)| \le \exp\left(-\frac{k_1}{2}t\right)|e_1(0)| + \frac{2}{k_1}\sup_{0\le\tau\le t}|e_2(\tau)|. \tag{10}$$

Equation (10) guarantees that the relationship between e_1 and e_2 has the ISS property. From (8) and (10), the ISS property of the overall tracking error system is represented by (6). Thus the tracking error dynamics in (5) represent the serial interconnected system of the ISS system. ■

Note that from the ISS property (6), as $t \to \infty$

$$|e_1(\infty)| \le \frac{2}{k_1}\sup_{0\le\tau\le\infty}|e_2(\tau)| \le \frac{2}{k_1 k_2}\sup_{0\le\tau\le\infty}|\tilde{d}(\tau)|. \tag{11}$$

B. AUGMENTED OBSERVER DESIGN

In this section, the augmented observer is designed to estimate the unmeasured state and unknown disturbance. By designing an augmented observer, the backstepping controller can compensate for the effect of unknown disturbances. Let us define an augmented state, x_a and its observer state, $\hat{x}_a$ as

$$x_a = \begin{bmatrix}x_1 & x_2 & x_3\end{bmatrix}^T,\ \hat{x}_a = \begin{bmatrix}\hat{x}_1 & \hat{x}_2 & \hat{x}_3\end{bmatrix}^T. \tag{12}$$

We assume that the disturbance of the given system varies slowly. With this assumption, the dynamics of d are represented as the following unknown nonlinear function $\kappa(\cdot)$:

$$\dot{d} = \kappa(x_a, t). \tag{13}$$

The dynamics of augmented observer can be written as

$$\dot{\hat{x}}_a = A_o\hat{x}_a + B_o u + B_\varphi\varphi + L_o C_o\left(x_a - \hat{x}_a\right) \tag{14}$$

where

$$A_o = \begin{bmatrix}0 & 1 & 0\\ 0 & 0 & 1\\ 0 & 0 & 0\end{bmatrix},\ B_o = \begin{bmatrix}0\\ g\\ 0\end{bmatrix},\ L_o = \begin{bmatrix}l_1\\ l_2\\ l_3\end{bmatrix}.$$

Here, C_o denotes the measurement matrix depending on the sensor configuration. φ and B_φ represent additional available external signals and matrice depending on the system.

Let us define the estimated error as $\tilde{x}_a = x_a - \hat{x}_a$. Then, the estimated state error dynamics become

$$\dot{\tilde{x}}_a = \left(A_o - L_o C_a\right)\tilde{x}_a - B_d\kappa \tag{15}$$

where $B_d = \begin{bmatrix}0 & 0 & 1\end{bmatrix}^T$. In this paper, we assume that the values of disturbances in the system are physically bounded. Therefore, κ is numerically bounded. In addition, there exists an unknown positive upper boundedness κ_{max} of $|\kappa|$ such that $\left|\dot{d}\right| = |\kappa| \le \kappa_{\max}$.

By substituting x by $\hat{x}$ in (4), we get

$$\begin{aligned}x_{2_d} &= -k_1\hat{e}_1 + \dot{x}_{1_d},\\ \hat{u} &= \frac{1}{g}\left(-k_2\hat{e}_2 + \dot{x}_{2_d} - \hat{d}\right)\end{aligned} \tag{16}$$

where $\hat{e}_i = \hat{x}_i - x_{i_d}$. Equation (16) is incorporated in (30) instead of (4). Consequently, substituting the estimated state and disturbance yield the following tracking error dynamics

$$\dot{e} = A_e e + B_e\tilde{\xi} \tag{17}$$

where

$$A_e = \begin{bmatrix}-k_1 & 1\\ 0 & -k_2\end{bmatrix}, B_e = \begin{bmatrix}0\\ 1\end{bmatrix},$$
$$\xi = d - \hat{d} + g\hat{u} - gu.$$

The overall closed-loop system becomes

$$\begin{aligned}\dot{e} &= A_e e + B_e \tilde{\xi} \\ \dot{\tilde{x}}_a &= A_o \tilde{x}_a + B_d \kappa.\end{aligned} \tag{18}$$

There exists $\gamma > 0$ such that

$$\left| d - \hat{d} + g\hat{u} - gu \right| \leq \gamma \|x_a - \hat{x}_a\|. \tag{19}$$

Theorem 2: The tracking error dynamics (17) have the ISS property such that

$$|e_1(t)| \leq \exp\left(-\frac{k_1}{2}t\right)|e_1(0)| + \frac{2}{k_1}\sup_{0\leq\tau\leq t}|e_2(\tau)|$$

and

$$|e_2(t)| \leq \exp\left(-\frac{k_2}{2}t\right)|e_2(0)| + \frac{2\gamma}{k_2}\sup_{0\leq\tau\leq t}\|\tilde{x}_a(\tau)\|. \tag{20}$$

◇

Proof: In (5), the e_2 dynamics are written as

$$\dot{e}_2 = -k_2 e_2 + d - \hat{d} + g\hat{u} - gu. \tag{21}$$

Then, we have

$$\frac{d}{dt}\left(\frac{e_2^2}{2}\right) \leq -\tfrac{k_2}{2}e_2^2 - \left(\tfrac{k_2}{2}\right)|e_2|\left(|e_2| - \sigma_1\right). \tag{22}$$

where $\sigma_1 = 2(|d - \hat{d} + g\hat{u} - gu|)/k_2$. From (19), we have

$$\sigma_1 = \frac{2|d - \hat{d} + g\hat{u} - gu|}{k_2} \leq \frac{2\gamma\|\tilde{x}_a\|}{k_2}. \tag{23}$$

Equation (8) is then rewritten as

$$|e_2(t)| \leq \exp\left(-\frac{k_2}{2}t\right)|e_2(0)| + \frac{2\gamma}{k_2}\sup_{0\leq\tau\leq t}\|\tilde{x}_a(\tau)\|. \tag{24}$$

■

III. CASCADE APPROACH

Let us consider the cascade system depicted in Fig. 1. The overall dynamics can be represented as follows:

$$\begin{aligned}{}^s\dot{e}_1 &= {}^s e_2 + {}^s x_{2_d} - {}^s\dot{x}_{1_d} \\ {}^s\dot{e}_2 &= g^s u + {}^s d - {}^s\dot{x}_{2_d}.\end{aligned} \tag{25}$$

where the superscript $s \in \{i, o\}$ denotes the inner-loop and outer-loop, respectively. Here, the input signal of the outer-loop, ${}^o\hat{u}$, becomes the desired value of the inner-loop. The actual input of the outer-loop system becomes the output signal of the inner-loop. Further, the actual input of the outer-loop that includes the error, ${}^o\hat{u}_a$, can be represented as follows:

$${}^o\hat{u}_a = {}^i x_1 = {}^i x_{1_d} + {}^i e_1. \tag{26}$$

From (3), the outer-loop and inner-loop of the cascade system can be represented as follows:

- Outer-loop

$$\begin{aligned}{}^o\dot{e}_1 &= {}^o e_2 + {}^o x_{2_d} - {}^o\dot{x}_{1_d} \\ {}^o\dot{e}_2 &= g^o u_a + {}^o d - {}^o\dot{x}_{2_d}.\end{aligned} \tag{27}$$

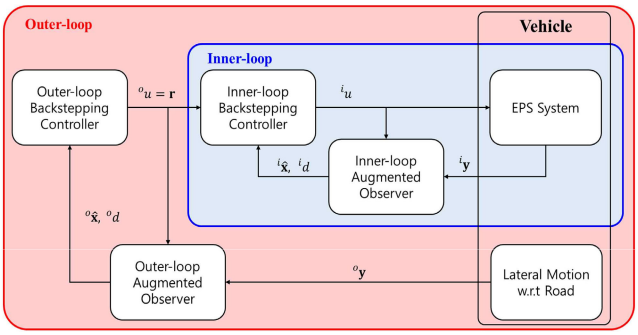

FIGURE 1. Cascade backstepping structure.

- Inner-loop

$$\begin{aligned}{}^i\dot{e}_1 &= {}^i e_2 + {}^i x_{2_d} - {}^i\dot{x}_{1_d} \\ {}^i\dot{e}_2 &= g^i u + {}^i d - {}^i\dot{x}_{2_d}.\end{aligned} \tag{28}$$

Here, the outer-loop dynamic equation e_2 becomes

$$\begin{aligned}{}^o\dot{e}_2 &= g^o u_a + {}^o d - {}^o\dot{x}_{2_d} \\ &= g\left({}^i x_{1_d} + {}^i e_1\right) + {}^o d - {}^o\dot{x}_{2_d} \\ &= g\left({}^o u + {}^i e_1\right) + {}^o d - {}^o\dot{x}_{2_d}.\end{aligned} \tag{29}$$

Applying the control law (4) yields the following equation:

$$\begin{aligned}{}^o\dot{e}_2 &= g\left({}^o u + {}^i e_1\right) + {}^o d - {}^o\dot{x}_{2_d} \\ &= -k_2{}^o e_2 + {}^o\tilde{d} + g^i e_1.\end{aligned} \tag{30}$$

Now we can represent the overall cascade system as follows with the backstepping controller (4)

$$\begin{aligned}{}^o\dot{e}_1 &= -k_1{}^o e_1 + {}^o e_2 \\ {}^o\dot{e}_2 &= -k_2{}^o e_2 + {}^o\tilde{d} + g^i e_1 \\ {}^i\dot{e}_1 &= -k_3{}^i e_1 + {}^i e_2 \\ {}^i\dot{e}_2 &= -k_4{}^i e_2 + {}^i\tilde{d}.\end{aligned} \tag{31}$$

Note that ${}^o\tilde{d} + g^i e_1$ is bounded because both ${}^i e_1$ and g are bounded. Then,

$$|{}^o e_2(t)| \leq \exp\left(-\frac{k_2}{2}t\right)|{}^o e_2(0)| + \frac{2}{k_2}\sup_{0\leq\tau\leq t}|\rho(\tau)| \tag{32}$$

where $\rho = {}^o\tilde{d} + g^i e_1$.

Finally, the tracking error dynamics (31) represent the serial interconnected system with the following ISS property from **Theorem 1**.

$$\begin{aligned}|{}^o e_1(t)| &\leq \exp\left(-\frac{k_1}{2}t\right)|{}^o e_1(0)| + \frac{2}{k_1}\sup_{0\leq\tau\leq t}|{}^o e_2(\tau)| \\ |{}^o e_2(t)| &\leq \exp\left(-\frac{k_2}{2}t\right)|{}^o e_2(0)| + \sup_{0\leq\tau\leq t}\sigma(\tau) \\ |{}^i e_1(t)| &\leq \exp\left(-\frac{k_3}{2}t\right)|{}^i e_1(0)| + \frac{2}{k_3}\sup_{0\leq\tau\leq t}|{}^i e_2(\tau)|\end{aligned}$$

$$|^i e_2(t)| \leq \exp\left(-\frac{k_4}{2}t\right)|^i e_2(0)| + \sup_{0\leq\tau\leq t}\rho(\tau) \tag{33}$$

where $\sigma = 2(|d - \hat{d} + g\hat{u} - gu|)/k_2$.

IV. APPLICATION

In this paper, we applied the proposed cascade control to the lateral control of autonomous vehicles such as in a lane keeping system (LKS). Lateral control of the vehicle is composed of an upper (outer) controller LKS to follow the given path, and a lower (inner) EPS controller to follow the target steering angle from the upper controller. The simplified second-order model for applying the proposed controller is covered in the next section.

A. INNER-LOOP ELECTRIC POWER STEERING SYSTEM

We consider a column-mounted EPS (C-EPS) system shown in Fig. 2. The C-EPS dynamic model can be represented with motor dynamics and a rack-bar motion dynamics as

$$J_m\ddot{\theta}_m + B_m\dot{\theta}_m = \tau - \tau_l \tag{34}$$

$$M_r\ddot{x}_r + B_r\dot{x}_r + K_r x_r = \frac{\tau_p}{R_p} - F_r. \tag{35}$$

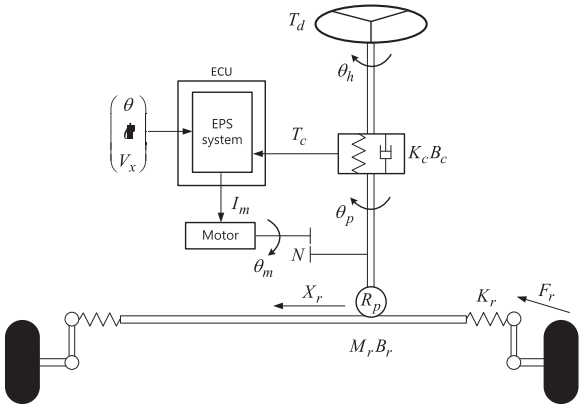

FIGURE 2. Diagram of EPS.

Further we have the following torque equation at the pinion

$$\tau_p = K_h\left(\theta_h - \frac{\theta_m}{N}\right) + N\tau_l. \tag{36}$$

To represent the EPS model in a second-order form, we assume that the steering column is considerable rigid. Then, we have $\theta_m = N\theta_p$ between the motor and pinion with the gear ratio, N. In addition, it can be assumed that the relation between the rack bar, x_r and the rotation of pinion, θ_p, is linear, i.e., $\theta_p = \frac{1}{R_p}x_r$ with (34), (35) and (36). Consequently, the second-order C-EPS dynamics can be modeled as:

$$\begin{aligned}\dot{\theta}_m &= \omega_m \\ \ddot{\theta}_m &= -\frac{B_{eq}}{J_{eq}}\dot{\theta}_m - \frac{K_{eq}}{J_{eq}}\theta_m + \frac{K_h}{J_{eq}N}\theta_h - \frac{R_p}{J_{eq}N}F_r + \frac{1}{J_{eq}}u\end{aligned} \tag{37}$$

where u is the input torque. Here, F_r is the load force applied to the rack bar in Fig. 2. We define the following parameters for the readability of the dynamic equation:

$$\begin{aligned}J_{eq} &= J_m + \frac{M_r {R_p}^2}{N^2},\ B_{eq} = B_m + \frac{B_r {R_p}^2}{N^2}, \\ K_{eq} &= \frac{K_r {R_p}^2}{N^2} + \frac{K_h}{N^2}\end{aligned} \tag{38}$$

where ${}^i x = [\theta_m \ \ \omega_m]^T$, $a_{21} = -\frac{K_{eq}}{J_{eq}}$, $a_{22} = -\frac{B_{eq}}{J_{eq}}$, $b_1 = \frac{1}{J_{eq}}$, $b_2 = -\frac{R_p}{J_{eq}N}$ and $b_3 = \frac{K_h}{J_{eq}N}$.

Consequently, the inner-loop second-order dynamics of EPS is given by

$$\begin{aligned}{}^i\dot{x}_1 &= {}^i x_2 \\ {}^i\dot{x}_2 &= b_1{}^i u + {}^i d\end{aligned} \tag{39}$$

where

$${}^i d = a_{21}{}^i x_1 + a_{22}{}^i x_2 + b_2 F_r + b_3\theta_h. \tag{40}$$

Here, the subscript i denotes the inner-loop. Now we can implement the proposed controller (4) using a simplified second-order EPS model (39).

B. OUTER-LOOP VEHICLE LATERAL MOTION MODEL

In this section, a simplified second-order dynamic model of the vehicle is derived using the well-known bicycle model. The bicycle model is used for lateral vehicle dynamics [20], as described in Fig. 3. The equation for lateral motion is

$$m(\ddot{y} + rV_x) = F_{yf} + F_{yr} \tag{41}$$

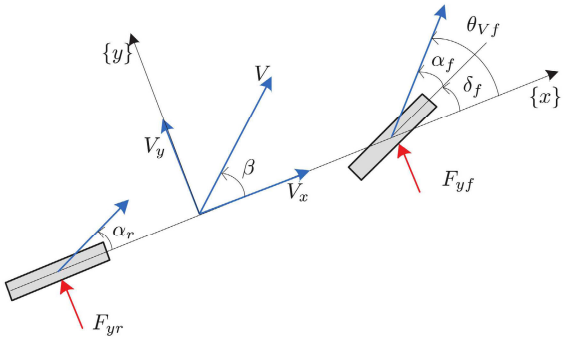

FIGURE 3. Bicycle model of the vehicle for lateral dynamics.

where

$$\begin{aligned}F_{yf} &= 2C_{\alpha f}\left(-\frac{\dot{y} + l_f r}{V_x}\right) \\ F_{yr} &= 2C_{\alpha r}\left(-\frac{\dot{y} + l_r r}{V_x}\right).\end{aligned}$$

In addition, the equation for the yaw dynamics is described as

$$I_z\dot{r} = M_z. \tag{42}$$

To track the desired lane on the road, both the lateral position error and heading angle with respect to the road are defined as follows

$$\begin{aligned} e_y &= y - y_d \\ e_\psi &= \psi - \psi_d. \end{aligned} \tag{43}$$

Then, from (43)

$$\begin{aligned} \ddot{e}_y &= \ddot{y} - \ddot{y}_d \\ &= a_{22}e_y + a_{23}e_\psi + a_{24}\dot{e}_\psi + b_{21}u + (-V_x + a_{24})\dot{\psi}_d \\ \ddot{e}_\psi &= \dot{\psi} - \dot{\psi}_d \\ &= a_{42}e_y + a_{43}e_\psi + a_{42}\dot{e}_\psi + b_{41}u + a_{44}\dot{\psi}_d. \end{aligned} \tag{44}$$

Now, let us define outer-loop state ${}^o x = \left[{}^o x_1 \ {}^o x_2\right]^T$ as follows [14]:

$$\begin{aligned} {}^o x_1 &= e_y + L e_\psi \\ {}^o x_2 &= \dot{e}_y + L \dot{e}_\psi \end{aligned} \tag{45}$$

where the superscript o denotes the outer-loop, ${}^o x_1$ is the lateral offset error at the look-ahead distance and ${}^o x_2$ is the derivative of ${}^o x_1$. The look-ahead distance L should be chosen considering the longitudinal velocity and maximum road curvature. We can obtain the dynamic of ${}^o x_2$ with constant velocity using (44) and (45) as follows:

$$\begin{aligned} {}^o\dot{x}_2 &= \ddot{e}_y + L\ddot{e}_\psi \\ &= (a_{22} + La_{42})\dot{e}_y + (a_{23} + La_{43})e_\psi + (a_{24} + La_{44})\dot{e}_\psi \\ &\quad + (a_{24} + La_{44} - V_x)\dot{\psi}_{des} + (b_{21} + Lb_{41})u. \end{aligned} \tag{46}$$

Consequently, the second order dynamics for lateral control are given by

$$\begin{aligned} {}^o\dot{x}_1 &= {}^o x_2 \\ {}^o\dot{x}_2 &= g_o {}^o u + {}^o d \end{aligned} \tag{47}$$

where

$$\begin{aligned} g_o &= b_{21} + Lb_{41} \\ d &= (a_{22} + La_{42})\dot{e}_y + (a_{23} + La_{43})e_\psi + (a_{24} + La_{44})\dot{e}_\psi \\ &\quad + (a_{24} + La_{44} - V_x)\dot{\psi}_{des}. \end{aligned} \tag{48}$$

Here, the convergence of ${}^o x_1$ and ${}^o x_2$ guarantees that both e_y and e_ψ are uniformly and ultimately bounded [14]. In other words, an LKS that satisfies the bounded error even with a simple second-order vehicle model can be designed. Finally, a cascade backstepping controller with an augmented observer using an inner-loop (39) and outer-loop (47) can be designed.

V. COMPUTATIONAL SIMULATIONS

A. SIMULATION SETUP

In the simulations, both the dynamic vehicle model in CarSim and the 4th-order nominal EPS model in [21] were used to validate the proposed algorithm. The proposed controller based on a simplified second-order model was implemented via MATLAB/Simulink. The sample times of the inner-loop EPS model and the outer-loop vehicle model were 10 ms and 100 ms, respectively. The parameters of a C-class hatchback in CarSim were used for the vehicle controller.

We applied a sine function with a magnitude of 5 Nm as the inner-loop EPS disturbance in consideration of the driver's disturbance and the uncertainty of system parameters. In addition, we considered that the difference between CarSim which contains high-order vehicle dynamics, and the simplified second-order model is the disturbance of the outer-loop vehicle model. Fig. 4 shows the reference roads for the high-speed and low-speed simulations, where the vehicle traveled at speeds of 80 km/h and 30 km/h, respectively. In this simulation, we set two different fixed look-ahead distances ($L = 1$ m for 80 km/h and $L = 4$ m for 30 km/h) for two cases depending on the longitudinal velocity and maximum road curvature. For comparison, the previous method (denoted as BTSP+BLF), which consists of barrier Lyapunov function (BLF) algorithm [22] for the outer-loop system and a backstepping controller for the inner-loop system was used. We can verify the lane keeping performance of the proposed algorithm through lateral offset error and heading angle error.

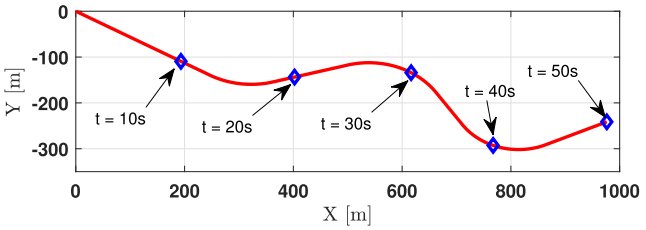

(a) Reference road for high speed case (80 km/h)

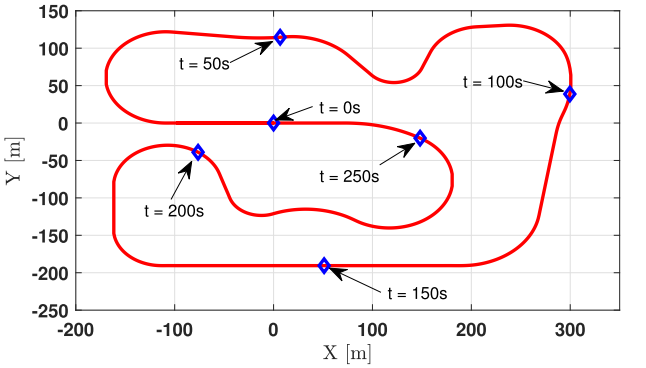

(b) Reference road for low speed case (30 km/h)

FIGURE 4. Reference roads for both cases.

B. RESULTS OF HIGH-SPEED CASE, 80 KM/H

The estimation performance of the proposed method for the high speed case is shown in Fig. 5. The overall state of the inner-loop system is shown in Fig. 5(a). Here, ${}^i x_1$ denotes the motor angle, ${}^i x_2$ denotes the rate of the motor angle, and ${}^i x_3$ denotes the disturbance of the EPS. The proposed augmented observer shows reasonable performance in the estimation of ${}^i x_1$. It is also evident that the motor angle ${}^i x_1$ changed as the vehicle entered the curved road at 12 s. The

steering wheel angle at the first curve was approximately 15°. Owing to the difference between the 4th-order steering model for the EPS system and the 2nd-order steering model for the controller, there was a disturbance when the vehicle entered or exited the curved road. Note that the disturbance also included the sinusoidal disturbances that we added.

In Fig. 5(b), the state of the outer-loop system is described. Here, ${}^{o}x_1$ denotes the lateral offset at the look-ahead distance, ${}^{o}x_2$ denotes its rate, and ${}^{o}x_3$ denotes disturbance of lateral dynamics. In particular, ${}^{o}x_3$ includes the nonlinear characteristics of vehicle dynamics and the parameter uncertainties. The estimation of ${}^{o}x_1$ is found to be highly accurate. The nonlinearity of the vehicle increases as the radius of curvature decreases. This nonlinearity became a disturbance for the second-order lateral dynamics. We observe that the magnitude of the disturbance increases when the vehicle travels on a curved road.

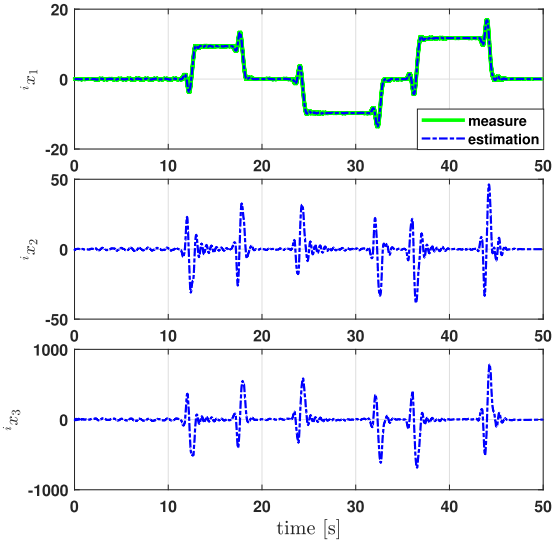

(a) State variables of inner-loop EPS system

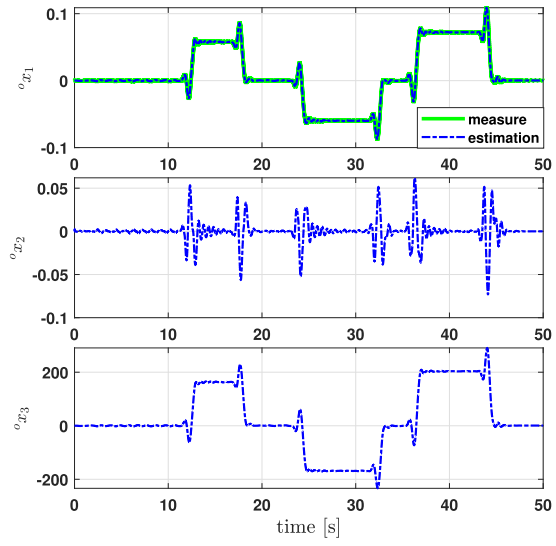

(b) State variables of outer-loop lateral dynamics

FIGURE 5. Estimation performance of proposed method for the high speed case.

The lane keeping performances of both the proposed method and the previous method can be validated using Fig. 6. The tracking errors of both methods are shown in Fig. 6(a). The proposed method maintained the vehicle at the center of the lane within approximately $e_y = \pm 0.1$ m. In addition, the maximum absolute value of the heading angle error was less than 0.012 rad on a severe curved road. In the high-speed simulation, the road radius gradually decreased. The difference between the lateral control performances of the two methods is the evident when the curvature of the road was the most severe at 45 s. Near 45 s, the tracking errors of the previous method increased compared to the proposed method. Furthermore, the oscillations occurred. At the end of the curve, the proposed method shows a more stable response without oscillations. On the other hand, the previous method had oscillations. Consequently, the input of the previous method also had oscillations compared to the proposed method as shown in Fig. 6(b). The yaw rate and lateral acceleration of the vehicle during the simulation are depicted in Fig. 6(c) We confirmed that even if disturbances occur in the inner and outer systems, the proposed algorithm achieves stable and reasonable lane keeping performance unlike the previous method.

C. RESULT OF LOW-SPEED CASE, 30 KM/H

The estimation performance of the proposed method for the low speed case is shown in Fig. 7. The overall state of the inner-loop system is shown in Fig. 7(a). The proposed augmented observer shows reasonable performance in the estimation of ${}^{i}x_1$. The motor angle ${}^{i}x_1$ changed as the vehicle entered the curved road at 12 s. The steering wheel angle at the first curve was approximately 35°. Owing to the difference between the 4th-order steering model for EPS system and the 2nd-order steering model for controller, there was a disturbance when the vehicle entered or exited the curved road. Note that the disturbance also included the sinusoidal disturbances that we added.

In Fig. 7(b), the state of the outer-loop system is described. In particular, ${}^{o}x_3$ includes the nonlinear characteristics of vehicle dynamics and parameter uncertainties. The estimation of ${}^{o}x_1$ was found to be highly accurate. The nonlinearity of the vehicle increases as the radius of curvature decreases. This nonlinearity became a disturbance for the second-order lateral dynamics. We observed that the magnitude of the disturbance increases when the vehicle travels on a curved road.

The lane keeping performances of both the proposed method and the previous method can be validated through Fig. 8. The tracking errors of both methods are shown in Fig. 8(a).

The proposed method maintained the vehicle at the center of the lane within approximately $e_y = \pm 0.1$ m. In addition, the maximum absolute value of the heading angle

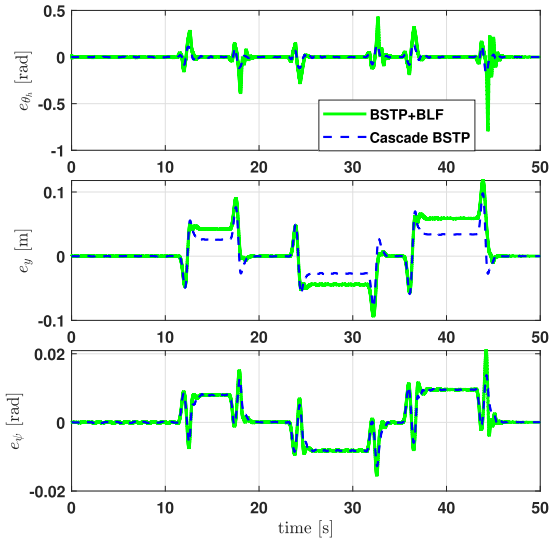

(a) Tracking errors

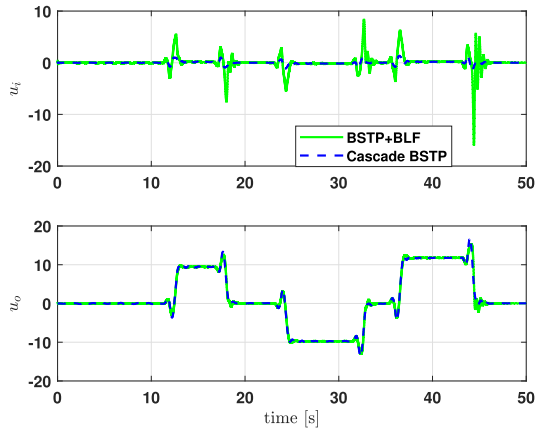

(b) Inputs

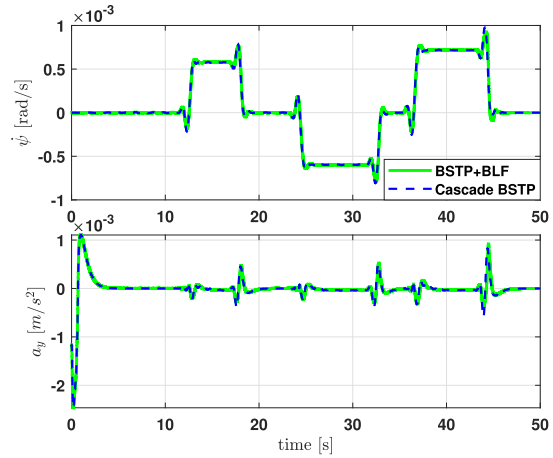

(c) Vehicle information

FIGURE 6. Lateral control performance of proposed and previous methods for the high speed case.

error was less than 0.2 rad on a severe curved road. In the low-speed simulation, the road radius continuously varied.

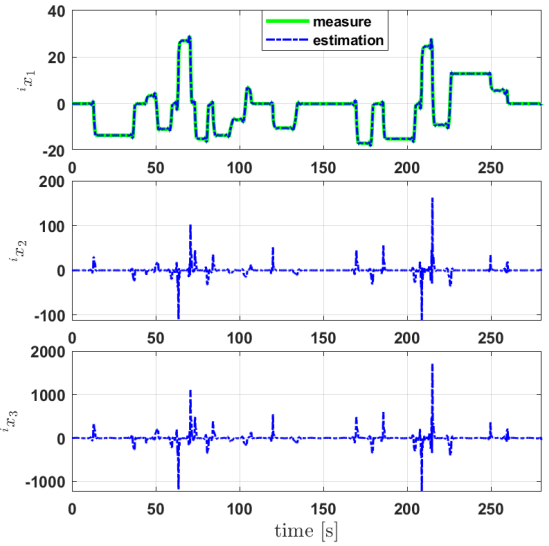

(a) State variables of inner-loop EPS system

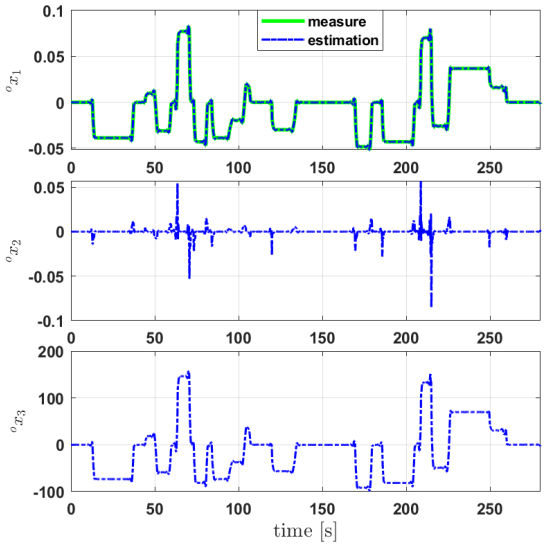

(b) State variables of outer-loop lateral dynamics

FIGURE 7. Estimation performance of proposed method for the low speed case.

The difference between the lateral control performances of the two methods is evident where the road curve was relatively severe from 60 s to 69 s and from 208 s to 213 s. From 60 s to 69 s and from 208 s to 213 s, the tracking errors of the proposed method were less than those of the previous method. Furthermore, the input of the previous method also had oscillations compared to the proposed method as shown in Fig. 8(b). The yaw rate and lateral acceleration of the vehicle during the simulation are depicted in Fig. 8(c). We confirmed that, even if disturbances occur in the inner and outer systems, the proposed algorithm achieved stable and reasonable lane-keeping performance, unlike the previous method.

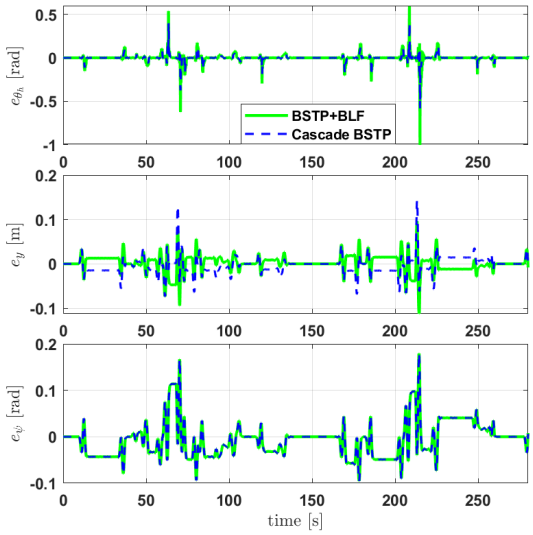

(a) Tracking errors

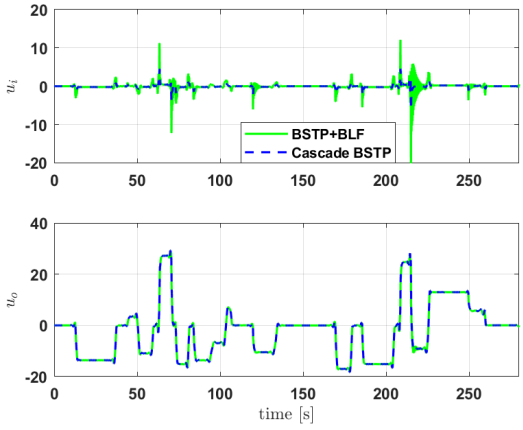

(b) Inputs

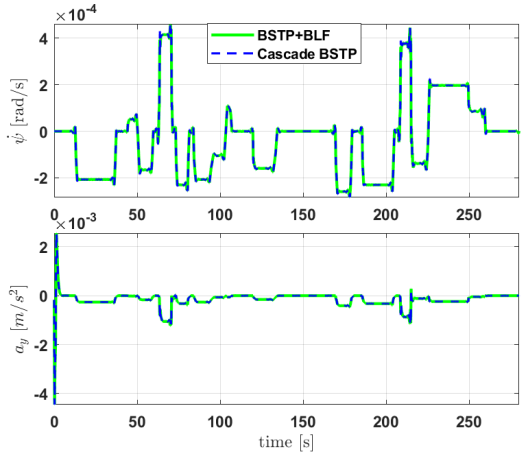

(c) Vehicle information

FIGURE 8. Lateral control performance of proposed and previous methods for the low speed case.

VI. CONCLUSION

In this paper, we proposed a cascaded backstepping control method with an augmented observer for the lateral control of an autonomous vehicle. The proposed method was designed to improve the lateral control performance, while guaranteeing the stability of the overall system via a cascaded backstepping procedure. The proposed method consists of an outer-loop controller for lateral dynamics and an inner-loop controller for the EPS system. Augmented observers were implemented in both the outer-loop and inner-loop controllers to improve robustness against unknown model parameters and external disturbances. Through simulations, it was shown that the proposed method guaranteed stability and improved lateral control performance under unknown model parameters and external disturbances. In future works, we plan to study lateral control methods by considering the time delay owing to communication.

REFERENCES

[1] J. Zhang and P. Ioannou, "Longitudinal control of heavy trucks in mixed traffic: Environmental and fuel economy considerations," *IEEE Trans. Intell. Transp. Syst.*, vol. 7, no. 1, pp. 92–104, Mar. 2006.

[2] C.-Y. Liang and H. Peng, "String stability analysis of adaptive cruise controlled vehicles," *JSME Int. J. C Mech. Syst. Mach. Elements Manuf.*, vol. 43, no. 3, pp. 671–677, 2000.

[3] B. Besselink and K. H. Johansson, "String stability and a delay-based spacing policy for vehicle platoons subject to disturbances," *IEEE Trans. Autom. Control*, vol. 62, no. 9, pp. 4376–4391, Sep. 2017.

[4] G. J. L. Naus, R. P. A. Vugts, J. Ploeg, M. J. G. van de Molengraft, and M. Steinbuch, "String-stable CACC design and experimental validation: A frequency-domain approach," *IEEE Trans. Veh. Technol.*, vol. 59, no. 9, pp. 4268–4279, Nov. 2010.

[5] S. Li, K. Li, R. Rajamani, and J. Wang, "Model predictive multi-objective vehicular adaptive cruise control," *IEEE Trans. Control Syst. Technol.*, vol. 19, no. 3, pp. 556–566, May 2011.

[6] Y. Luo, T. Chen, S. Zhang, and K. Li, "Intelligent hybrid electric vehicle ACC with coordinated control of tracking ability, fuel economy, and ride comfort," *IEEE Trans. Intell. Transp. Syst.*, vol. 16, no. 4, pp. 2303–2308, Aug. 2015.

[7] G. V. Raffo, G. K. Gomes, J. E. Normey-Rico, C. R. Kelber, and L. B. Becker, "A predictive controller for autonomous vehicle path tracking," *IEEE Trans. Intell. Transp. Syst.*, vol. 10, no. 1, pp. 92–102, Mar. 2009.

[8] C. M. Kang, S.-H. Lee, and C. C. Chung, "On-road path generation and control for waypoints tracking," *IEEE Trans. Intell. Transp. Syst. Mag.*, vol. 9, no. 3, pp. 36–45, Jul. 2017.

[9] C. M. Kang, S.-H. Lee, and C. C. Chung, "Multirate lane-keeping system with kinematic vehicle model," *IEEE Trans. Veh. Technol.*, vol. 67, no. 10, pp. 9211–9222, Oct. 2018.

[10] J. E. Naranjo, C. Gonzalez, R. Garcia, and T. de Pedro, "Lane-change fuzzy control in autonomous vehicles for the overtaking maneuver," *IEEE Trans. Intell. Transp. Syst.*, vol. 9, no. 3, pp. 438–450, Sep. 2008.

[11] T. Hessburg and M. Tomizuka, "Fuzzy logic control for lateral vehicle guidance," *IEEE Control Syst.*, vol. 14, no. 4, pp. 55–63, Aug. 1994.

[12] X. Jin, Z. Yu, G. Yin, and J. Wang, "Improving vehicle handling stability based on combined AFS and DYC system via robust Takagi-Sugeno fuzzy control," *IEEE Trans. Intell. Transp. Syst.*, vol. 19, no. 8, pp. 2696–2707, Aug. 2018.

[13] X. Jin, J. Yang, Y. Li, B. Zhu, J. Wang, and G. Yin, "Online estimation of inertial parameter for lightweight electric vehicle using dual unscented Kalman filter approach," *IET Intell. Transp. Syst.*, vol. 14, no. 5, pp. 412–422, 2020.

[14] C. M. Kang, W. Kim, and C. C. Chung, "Observer-based backstepping control method using reduced lateral dynamics for autonomous lane-keeping system," *ISA Trans.*, vol. 83, pp. 214–226, Dec. 2018.

[15] Y. W. Jeong, C. C. Chung, and W. Kim, "Nonlinear hybrid impedance control for steering control of rack-mounted electric power steering in autonomous vehicles," *IEEE Trans. Intell. Transp. Syst.*, vol. 21, no. 7, pp. 2956–2965, Jul. 2020.

[16] F.-J. Lin, Y.-C. Hung, and K.-C. Ruan, "An intelligent second-order sliding-mode control for an electric power steering system using a wavelet fuzzy neural network," *IEEE Trans. Fuzzy Syst.*, vol. 22, no. 6, pp. 1598–1611, Dec. 2014.
[17] P. Falcone, F. Borrelli, J. Asgari, H. E. Tseng, and D. Hrovat, "Predictive active steering control for autonomous vehicle systems," *IEEE Trans. Control Syst. Technol.*, vol. 15, no. 3, pp. 566–580, May 2007.
[18] Z. He, L. Nie, Z. Yin, and S. Huang, "A two-layer controller for lateral path tracking control of autonomous vehicles," *Sensors*, vol. 20, no. 13, p. 3689, Jul. 2020, doi: 10.3390/s20133689.
[19] M. Krstic, I. Kanellakopoulos, and PV. Kokotovic, *Nonlinear and Adaptive Control Design*. Hoboken, NJ, USA: Wiley, 1995.
[20] R. Rajamani, *Vehicle Dynamics and Control*, 2nd ed. Cham, Switzerland: Springer, 2012.
[21] A. Marouf, M. Djemai, C. Sentouh, and P. Pudlo, "A new control strategy of an electric-power-assisted steering system," *IEEE Trans. Veh. Technol.*, vol. 61, no. 8, pp. 3574–3589, Oct. 2012.
[22] Y. Hwang, C. M. Kang, and W. Kim, "Robust nonlinear control using barrier Lyapunov function under lateral offset error constraint for lateral control of autonomous vehicles," *IEEE Trans. Intell. Transp. Syst.*, early access, Sep. 23, 2020, doi: 10.1109/TITS.2020.3023617.

CHANG MOOK KANG (Member, IEEE) received the B.S. and Ph.D. degrees in electrical engineering from Hanyang University (HYU), Seoul, South Korea, in 2012 and 2018, respectively. In 2018, he joined the Agency for Defense Development (ADD), Daejeon, South Korea, as a Senior Research Engineer, and was also a Senior Researcher with the Presidential Security Service (PSS), South Korea. He is currently an Assistant Professor with the Department of Electrical Engineering, Incheon National University (INU). His current research interests include control theory, unmanned systems, and reinforcement learning for autonomous driving. He is also a member of the IEEE Intelligent Transportation Systems Society (ITSS), the IEEE Control Systems Society, and the Institute of Control, Robotics and Systems (ICROS).

WONHEE KIM (Member, IEEE) received the B.S. and M.S. degrees in electrical and computer engineering and the Ph.D. degree in electrical engineering from Hanyang University, Seoul, South Korea, in 2003, 2005, and 2012, respectively.

From 2005 to 2007, he was with Samsung Electronics Company, Suwon, South Korea. In 2012, he was with the Power and Industrial Systems Research and Development Center, Hyosung Corporation, Seoul. In 2013, he was a Postdoctoral Researcher with the Institute of Nano Science and Technology, Hanyang University, and a Visiting Scholar with the Department of Mechanical Engineering, University of California, Berkeley, CA, USA. From 2014 to 2016, he was with the Department of Electrical Engineering, Dong-A University, Busan, South Korea. He is currently an Associate Professor with the School of Energy Systems Engineering, Chung-Ang University, Seoul. His current research interests include nonlinear control and nonlinear observers and their industrial applications. He has served as an Associate Editor for IEEE Access, IEEE/ASME Transactions on Mechatronics, and the *Journal of Electrical Engineering and Technology*.

HYEONGBOO BAEK received the B.S. degree in computer science and engineering from Konkuk University, South Korea, in 2010, and the M.S. and Ph.D. degrees in computer science from KAIST, South Korea, in 2012 and 2016, respectively. He is currently an Assistant Professor with the Department of Computer Science and Engineering, Incheon National University (INU), South Korea. His research interests include cyber physical systems, real time embedded systems, and system security. He won the Best Paper Award from the 33rd IEEE Real Time Systems Symposium (RTSS) in 2012.